Fuzzy Logic Control Using SVPWM to Enhance the Control of the DFIG Driven by a Wind Turbine

Abdelhalim Arif, **Youcef Bekakra**†, and **Djilani Ben Attous**, Non-members

ABSTRACT

The Fuzzy Logic Controller (FLC) is applied in this paper to enhance the control of a doubly fed induction generator (DFIG) driven by a wind turbine (WT) with the space vector pulse width modulation (SVPWM) inverter. The proposed model is then compared to a classical pulse width modulation (PWM) inverter to improve the quality of the generated energy. The simulation results of these two techniques are presented under MATLAB/Simulink. The results show that FLC-SVPWM gives a lower value for total harmonic distortion (THD) of the stator current as well as reduced ripples of active and reactive powers compared to the FLC-PWM.

Keywords: Wind Turbine, Doubly Fed Induction Generator, DFIG, Fuzzy Logic Control, Pulse Width Modulation, PWM, Space Vector Pulse Width Modulation, SVPWM

NOMENCLATURE

V_{sdq}, V_{rdq}	Stator and rotor voltages in dq frame (V)
i_{sdq}, i_{rdq}	Stator and rotor currents in dq frame (A)
ϕ_{sdq}, ϕ_{rdq}	Stator and rotor flux in dq frame (Wb)
P_s, Q_s	Stator active and reactive powers (W, Var)
C_e	Electromagnetic torque (N · m)
R_s, R_r	Stator and rotor resistances (Ω)
L_s, L_r	Stator and rotor inductances (H)
M	Magnetizing inductance (H)
σ	Coefficient of dispersion
g	Slip coefficient
ω_s, ω_r	Stator and rotor angular frequency (rad/s)
ρ	Air density
β	Blades pitch angle
λ	Tip speed ratio
C_p	Power coefficient
S_w	Area of wind turbine blades

1. INTRODUCTION

Wind is considered one of the most important energy sources in the world due to its cleanliness and its free and extensive availability in nature and lack of hostility to the environment [1]. With new offshore developments and the increasing installation of larger machines, wind turbine power has grown and expanded worldwide, reaching about 540 GW by the end of 2017, 18 GW being extracted offshore. Operation and maintenance are very important for the survival of wind turbines. However, the costs involved are high, reaching around 25% of the total costs of a wind farm. This percentage can rise to 35% for the maintenance and operation of advanced offshore wind turbines [2].

Doubly fed induction generator (DFIG) and permanent magnet synchronous generator (PMSG) wind power plants are growing in popularity and widely used for electrical power generation [3, 4]. This has led researchers to devise new control techniques to obtain the largest amount of electrical energy. Descriptions of some of these generators are presented and compared below:

- The DFIG operates over a limited speed range of ±30% synchronous speed by controlling its rotor using a back-to-back converter (rotor side converter (RSC)-DC Link-grid side converter (GSC)). This results in 100% of the total power and 30% of the rated power being absorbed by the rotor converters, while 70% of the rated power is injected directly into the grid. However, the PMSG operates on the self-excitation resulting from the permanent magnet in its rotor to obtain 100% of the total rated power in the stator passing through the power converters (machine side converter (MSC)-DC Link-GSC) to the grid, thus producing more harmonics for injection into the grid [5, 6].
- DFIG-based wind turbines require a gearbox to adapt the rotor speed with the turbine speed. Unlike PMSG-based wind turbines, it does not require a gearbox [7].
- The DFIG is known to provide constant amplitude and frequency for the stator voltage at a variable wind speed, which is directly proportional to the speed of its rotor controlled by a back-to-back converter (RSC-DC Link-GSC). However, in the PMSG, the amplitude and frequency of the stator voltage are directly proportional to the wind speed. Consequently, it cannot be integrated directly into the grid, except after passing through converters (MSC-DC Link-GSC).
- The power converters used to control the rotor of a DFIG are smaller, making it less expensive, with its capacity estimated to be 30% of the nominal power. However, the power converters (MSC-DC Link-GSC) used to control the stator of the PMSG are bigger in comparison to the DFIG, making it more expensive since its capacity is estimated according to the total

Manuscript received on August 7, 2020; revised on September 7, 2021; accepted on September 16, 2021. This paper was recommended by Associate Editor Kriangkrai Sooksood.

The authors are with the LEVRES Laboratory, University of El Oued, 39000 El Oued, Algeria.

†Corresponding author: youcef-bekakra@univ-eloued.dz

Digital Object Identifier: 10.37936/ecti-eec.2022201.241670

nominal power [8].

- The DFIG-based wind turbine ensures complete independence between active and reactive power control. It also provides high power for low wind sites by capturing the maximum power extraction available in the wind [8]. On the other hand, the wind turbine based on multi-pole PMSG is capable of producing higher torque at low wind speed. However, the multi-pole PMSG is big and heavy [6].
- The DFIG and PMSG provide complete control of both reactive and active power [6].

In view of its multiple features, this study focuses on the DFIG. It adapts well to variable wind speed and has the potential to control the active and reactive powers, power factor, and stator voltage simultaneously at its rotor side with a small amount of power.

The working principle of a wind turbine driven by wind current is based on rotating the DFIG rotor to obtain electrical energy in the stator. Wind turbines can be divided into two main types in terms of wind speed: a wind turbine driven by a fixed speed, and a wind turbine driven by a variable speed. Among the advantages of variable speed wind turbines compared to conventional fixed-speed wind turbines are that they can reduce fluctuation in electrical energy and increase energy capture, enhancing the dynamic behavior caused by mitigating mechanical stress. Such advantages contribute to improving the quantity and quality of energy generated [9].

In order to maximize the exploitation of wind energy, wind turbines must be directed to track the maximum power points at different wind speeds. The rotor speed of the DFIG should vary widely, to obtain the maximum possible energy (pursued in region 2) extracted from wind, and several maximum power point tracking technologies have been discovered. These technologies can be listed under three main types: optimal tip speed ratio (TSR), power signal feedback (PSF), and hill-climbing search (HCS) techniques [10].

The optimal TSR method is used to adjust the rotor speed of the DFIG to create the optimum value for the tip speed ratio, corresponding to the maximum energy extracted from wind turbines. This strategy requires the measurement or estimation of wind and turbine speed. It also requires knowledge of the optimum ratio for the turbine tip speed. With the provision of this data, the system can extract the maximum power points [11].

The PSF strategy is used to measure the angular velocity of a wind turbine. The mechanical output power of the wind turbine is adjusted according to the output power of the DFIG based on the maximum power curve of the wind turbine, enabling the maximum power points to be tracked. However, the difficulty involved in obtaining the maximum power curve of a wind turbine makes calculating the stator power of a DFIG complicated [12].

The HCS algorithm uses the search-remember-reuse process to store the maximum power points obtained during the training process. This strategy starts from an empty smart memory with relatively poor initial performance and is then gradually trained by an advanced hill-climbing search for data acquisition. This process is repeated until an accurate memory is created to deal with the characteristics of the system. The smart memory of this strategy is trained online to improve the performance of maximum power tracking [11]. Furthermore, the HCS strategy is considered to be the best of the three approaches because it does not require the measurement of wind speed or use the characteristic wind turbine power curve. It is sufficient to merely apply the rotor speed disturbance variation artificially. The rotor speed disturbance increment is obtained based on changes in the output power of wind turbines. The rotor speed is adjusted to the set value by varying the electromagnetic torque of the generator, and the process repeated until the maximum power point is obtained. This is managed with the use of a computer program [12].

In region 3 (full-load), the blade pitch angle (β) is controlled to reduce the effect of wind speed, which is higher than the maximum rated speed. The rated speed of the generator is maintained by reducing the aerodynamic energy applied to the blade along with the excess power, not only to avoid exceeding the rated power of the generator but also to maximize power point tracking efficiency [13]. In this region, the power coefficient (C_p) varies according to the change in pitch angle, unlike region 2 which is fixed at the maximum value.

Fuzzy logic originally appeared in 1965 [14], proposed by mathematical professor Zadeh from the University of California, Berkeley, but the idea did not take off at that time. In 1974, Mamdani, a senior professor at the University of London, applied the idea of fuzzy logic to control automatic steam engines, and since that time, the application and development of this idea have continued [15].

The aim of fuzzy logic is to achieve range-to-point or range-to-range control. Unlike the classical point-to-point control technique, the results from the fuzzy logic controller are derived for both inputs and outputs. They use each other's associated membership functions (MFs) by converting crisp input into linguistic variables based on their value. The output of the fuzzy logic controller depends on the degree of its membership in the various MFs, which could be considered as inputs [15].

In this paper, the fuzzy logic controller (FLC) is used to control the inverter on the rotor side, providing active and reactive powers with a lower ripple, greater efficiency, and stability during operation. The FLC can be distinguished from the conventional controller by being uncomplicated and easier to use on the computer, while the input has no proportional point-by-point relationship with output. Therefore, it can obtain stability in transient and non-linear systems by providing variable gains commensurate with the needs of the system [16].

Space vector pulse width modulation (SVPWM) is a successful inverter control technology for improving the performance of switching sequences when compared to

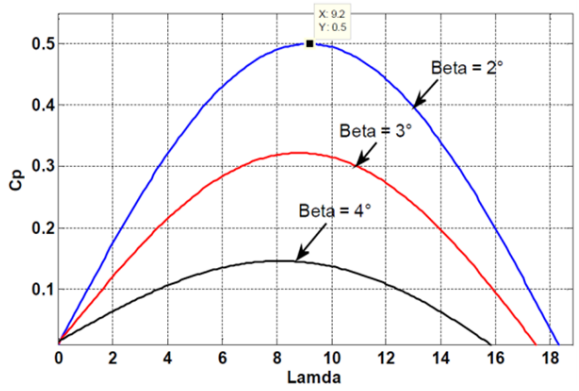

Fig. 1: Coefficient of power (C_p) as a function of λ and β.

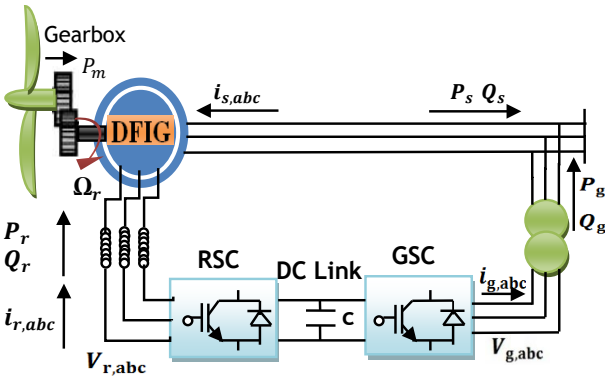

Fig. 2: General scheme of the DFIG driven by a wind turbine.

PWM. This improved performance provides lower ripples and lower THD.

The main contribution of this paper is summarized below:

- The FLC is used to avoid the drawbacks involved with conventional control because it is not related to the system model.
- The inverter is controlled by using the SVPWM technique to reduce the ripples of active and reactive powers that minimize the THD of the stator currents, improving the quality of generated energy.

2. TURBINE MODEL

The wind power sweeping through the turbine input is given by the following equation [17, 18]:

$$P_v = \frac{1}{2}\rho S_w v^3 \tag{1}$$

where ρ represents the air density, S_w represents the area of the wind turbine blades, and v represents the wind speed.

When the wind rotates the turbine, this results in mechanical power for the turbine, given by

$$P_m = C_p P_v = \frac{1}{2} C_p \rho S_w v^3 \tag{2}$$

where C_p is the coefficient of power, representing the efficiency of wind turbine energy conversion. The C_p changes as a function of λ and β as

$$C_p(\beta,\lambda) = [0.5-0.0167\cdot(\beta-2)]\cdot \sin\left(\frac{\pi\cdot(\lambda+0.1)}{18.5-0.3\cdot(\beta-2)}\right) - 0.00184\cdot(\lambda-3)\cdot(\beta-2) \tag{3}$$

where λ represents the tip speed ratio and β represents the blade pitch angle.

The tip speed of the turbine blades is given by

$$\lambda = \frac{R\Omega_t}{v} \tag{4}$$

where R represents the blade radius of the wind turbine and Ω_t represents the angular speed of the wind turbine.

Changes in the C_p as a function of λ and β are presented in Fig. 1.

3. DFIG MODEL

The DFIG is important for electrical power production since it can obtain pure and abundant electrical power from wind. To achieve this, the following devices must be provided: DFIG, WT with MPPT control strategy, and a back-to-back converter (RSC-DC Link-GSC). The rotor current of the DFIG can then be controlled by the RSC, as shown in Fig. 2 [19].

After transforming from the a, b, c to the d, q reference, the stator and rotor voltages are given below:

$$V_{sdq} = R_s i_{sdq} + \frac{d}{dt}\phi_{sdq} \mp \omega_s \phi_{sqd} \tag{5}$$

$$V_{rdq} = R_r i_{rdq} + \frac{d}{dt}\phi_{rdq} \mp (\omega_s - \omega_r)\phi_{rqd}. \tag{6}$$

The expressions of stator and rotor flux (dq-axis) are given as follows:

$$\phi_{sdq} = L_s i_{sdq} + M i_{rdq} \tag{7}$$

$$\phi_{rdq} = L_r i_{rdq} + M i_{sdq}. \tag{8}$$

The equations of active and reactive powers are given as follows:

$$P_s = V_{sd} i_{sd} + V_{sq} i_{sq} \tag{9}$$

$$Q_s = V_{sq} i_{sd} - V_{sd} i_{sq}. \tag{10}$$

The electromagnetic torque for the DFIG is given below:

$$C_e = pM\left(i_{rd}\cdot i_{sq} - i_{rq}\cdot i_{sd}\right). \tag{11}$$

4. DFIG CONTROL STRATEGY

The stator flux orientation strategy facilitates DFIG control, providing separate control of active and reactive powers. The principle of this technique is based on the stator flux aligning with all axis d points of the rotating frame. Fig. 3 shows the orientation of the d, q frame [5].

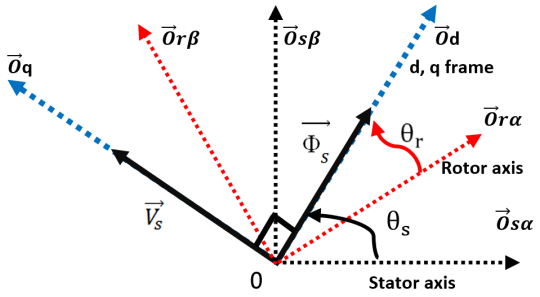

Fig. 3: Diagram of the d, q frame stator flux orientation.

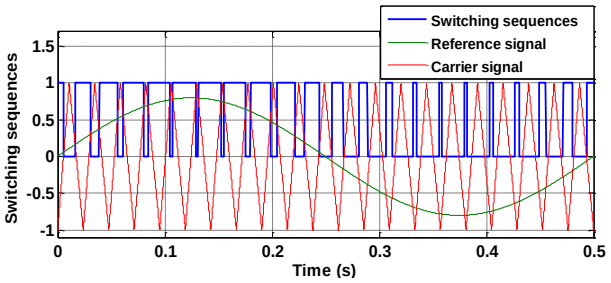

Fig. 4: Switching sequences using the classical PWM inverter.

By applying the stator flux orientation strategy shown in Fig. 3, the flux equations are presented as follows:

$$\phi_{sd} = \phi_s \tag{12}$$
$$\phi_{sq} = 0. \tag{13}$$

The new equations for stator voltages are

$$V_{sd} = 0 \tag{14}$$
$$V_{sq} = V_s = \omega_s \phi_s. \tag{15}$$

and for the rotor voltages

$$V_{rd} = R_r i_{rd} + \sigma L_r \frac{d}{dt} i_{rd} - g\omega_s \sigma L_r i_{rq} \tag{16}$$
$$V_{rq} = R_r i_{rq} + \sigma L_r \frac{d}{dt} i_{rq} + g\frac{M}{L_s} V_s + g\omega_s \sigma L_r i_{rd}. \tag{17}$$

The new equations of stator currents are shown as follows:

$$i_{sd} = -\frac{M}{L_s} i_{rd} + \frac{\phi_s}{L_s} \tag{18}$$
$$i_{sq} = -\frac{M}{L_s} i_{rq}. \tag{19}$$

The simplified equations of active and reactive powers are given as follows:

$$P_s = -V_s \frac{M}{L_s} i_{rq} \tag{20}$$
$$Q_s = \frac{V_s^2}{\omega_s L_s} - V_s \frac{M}{L_s} i_{rd}. \tag{21}$$

The simplified electromagnetic torque equation is given as follows:

$$C_e = -p\frac{M}{L_s} \phi_{sd} i_{rq}. \tag{22}$$

5. INVERTER CONTROL WITH PWM AND SVPWM

5.1 Classical PWM

Classical PWM is a conventional technique based on finding the difference between the reference and carrier signals. The carrier signal is characterized by the frequency being several times higher than the reference frequency. For example, it could be 21 times higher and its amplitude greater than or equal to that of the reference signal. This difference is passed in relay to determine the switching sequences, $(s_a,\ s_b,\ s_c) = (0, 1)$, as shown in Fig. 4.

5.2 Space Vector PWM (SVPWM)

One of the most effective and widespread techniques for controlling two-level and multi-level inverters is the SVPWM [20]. This is because of its flexibility in implementation on hardware and software and its ease of application onto computers. Moreover, it offers a relatively better control performance compared to the classical PWM because it contains a switching sequence that greatly affects the THD [21].

The SVPWM passes through five main stages, the first of which involves the calculation of v_α, v_β, and v_{ref}. The second stage concerns the calculation of the sector number, while in the third stage the dwell times are calculated. The fourth stage involves the calculation of the switching time signals, while during the final stage the switching sequences are calculated. These five stages are detailed as follows:

Stage 1: Calculation of voltage values v_α, v_β, and v_{ref}

To calculate the voltages v_α and v_β, Clarke transformation must be used to transform a three-phase plane (a, b, c) into a bi-phase plane (α, β). The matrix of this transformation is illustrated as follows:

$$\begin{bmatrix} v_\alpha \\ v_\beta \end{bmatrix} = \begin{bmatrix} 1 & -\frac{1}{2} & -\frac{1}{2} \\ 0 & \frac{\sqrt{3}}{2} & \frac{\sqrt{3}}{2} \end{bmatrix} \begin{bmatrix} v_a \\ v_b \\ v_c \end{bmatrix} \tag{23}$$

$$v_{ref} = \sqrt{v_\alpha^2 + v_\beta^2}. \tag{24}$$

Stage 2: Calculation of sector number

In order to determine the sector along the circle, the angle between v_α and v_β must be calculated, which is given as follows:

$$\theta = \arctan\left(\frac{v_\beta}{v_\alpha}\right). \tag{25}$$

Each sector is determined by the angle field, which

Table 1: *Sectors and switching states of the SVPWM.*

Sector	Switching States	Angle θ
1	$V_0, V_1, V_2, V_7, V_7, V_2, V_1, V_0$	$0° \le \theta < 60°$
2	$V_0, V_3, V_2, V_7, V_7, V_2, V_3, V_0$	$60° \le \theta < 120°$
3	$V_0, V_3, V_4, V_7, V_7, V_4, V_3, V_0$	$120° \le \theta < 180°$
4	$V_0, V_5, V_4, V_7, V_7, V_4, V_5, V_0$	$-180° \le \theta < -120°$
5	$V_0, V_5, V_6, V_7, V_7, V_6, V_5, V_0$	$-120° \le \theta < -60°$
6	$V_0, V_1, V_6, V_7, V_7, V_6, V_1, V_0$	$-60° \le \theta < 0°$

Table 2: *Calculation of the angle 'phi' using angle θ.*

Sector	S_1	S_2	S_3	S_4	S_5	S_6
phi	θ	$\theta - \frac{\pi}{3}$	$\theta - \frac{2\pi}{3}$	$\theta + \pi$	$\theta + \frac{2\pi}{3}$	$\theta + \frac{\pi}{3}$

Table 3: *Switching time signals.*

Sector	T_a	T_b	T_c
1	$T_1 + T_2 + \frac{T_0}{2}$	$T_2 + \frac{T_0}{2}$	$\frac{T_0}{2}$
2	$T_1 + \frac{T_0}{2}$	$T_1 + T_2 + \frac{T_0}{2}$	$\frac{T_0}{2}$
3	$\frac{T_0}{2}$	$T_1 + T_2 + \frac{T_0}{2}$	$T_2 + \frac{T_0}{2}$
4	$\frac{T_0}{2}$	$T_1 + \frac{T_0}{2}$	$T_1 + T_2 + \frac{T_0}{2}$
5	$T_2 + \frac{T_0}{2}$	$\frac{T_0}{2}$	$T_1 + T_2 + \frac{T_0}{2}$
6	$T_1 + T_2 + \frac{T_0}{2}$	$\frac{T_0}{2}$	$T_2 + \frac{T_0}{2}$

contains switching states, as shown in Table 1 and Fig. 5 [22].

Stage 3: Calculating the dwell times

In order to calculate the dwell times, the angle *phi* is initially considered, using angle θ and the sectors, as illustrated in Table 2. Based on the results presented in Table 2, the dwell times (T_1, T_2, T_0) can be calculated as follows:

$$T_1 = \frac{v_{ref} \cdot T \cdot \sin\left(\frac{\pi}{3} - phi\right)}{\frac{2}{3} \cdot V_{dc} \cdot \sin\left(\frac{\pi}{3}\right)} \tag{26}$$

$$T_2 = \frac{v_{ref} \cdot T \cdot \sin\left(phi\right)}{\frac{2}{3} \cdot V_{dc} \cdot \sin\left(\frac{\pi}{3}\right)} \tag{27}$$

$$T_0 = T - (T_1 + T_2) \tag{28}$$

Stage 4: Calculation of the switching time signals

Switching times can be calculated using the sectors and the dwell times shown in Table 3.

Stage 5: Calculation of switching sequences

This stage is designed to find the difference between the switching time and carrier signals. The carrier signal has a significantly higher frequency (as much as 21 times)

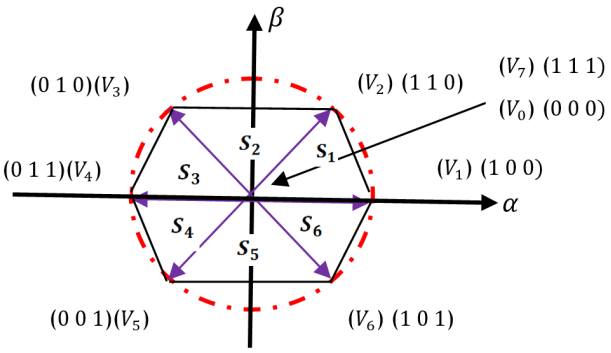

Fig. 5: *Diagram of hexagon switches.*

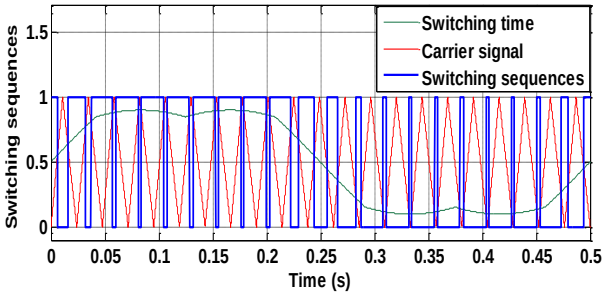

Fig. 6: *Switching sequences using SVPWM.*

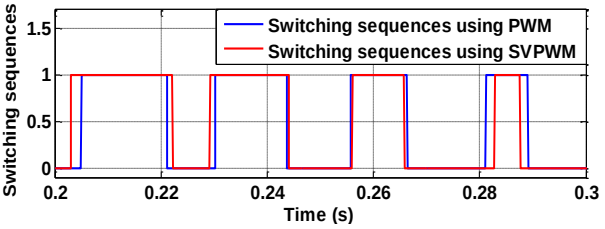

Fig. 7: *Switching sequences using PWM and SVPWM.*

than that of the reference, with an amplitude greater than or equal to the amplitude of the switching time signal. This difference is passed in relay to determine the switching sequences, $(s_a, s_b, s_c) = (0, 1)$, as shown in Fig. 6. The switching sequences using PWM and SVPWM are illustrated in Fig. 7.

6. FUZZY CONTROL OF THE DFIG

The fuzzy logic controller (FLC) is an advanced technology that can handle non-linear systems well. This technique is somewhat similar to the flexibility of human thinking, providing satisfactory performance and an approximate solution for complex and non-linear system problems which cannot be solved by the classical controller [5].

To properly implement the fuzzy logic controller strategy, the following three stages should be considered [15].

- **Fuzzification:** in this stage, the crisp data (error, error change) is converted into MFs or fuzzy data using the fuzzy system.
- **Fuzzy inference process:** in this stage, MFs or fuzzy

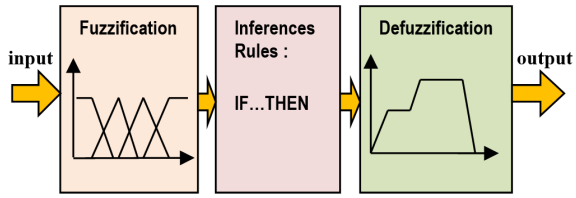

Fig. 8: *Diagram of fuzzy control stages.*

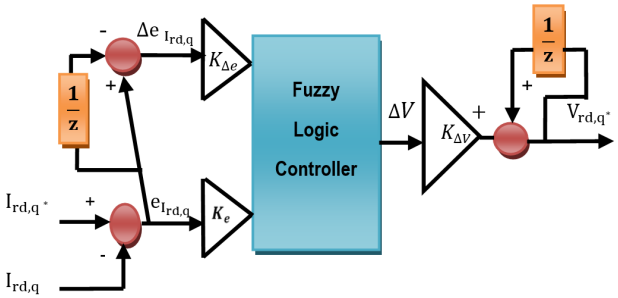

Fig. 9: *General model of the fuzzy logic controller.*

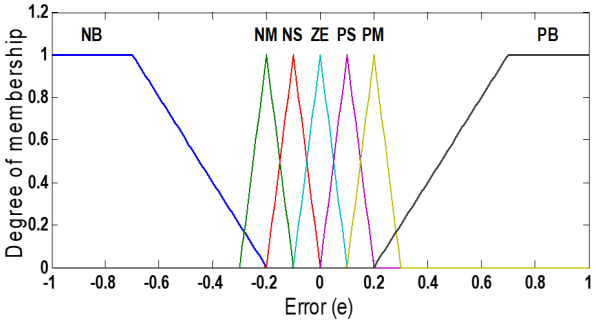

Fig. 10: *Membership functions of error.*

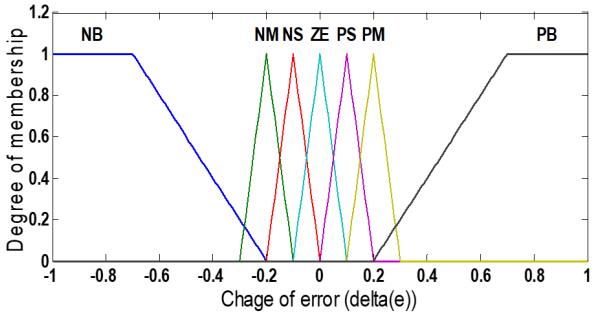

Fig. 11: *Membership functions of change of error (Δe).*

data are combined with inferential control rules such as the conditional rule (If....Then) to derive the fuzzy output.

- **Defuzzification:** in this stage, different methods are used to calculate the output associated with the MFs and enter it into the lookup table; the output from this table is then picked up based on the current input during the application.

These stages are shown in Fig. 8. The fuzzy logic studied in this paper is based on the Mamdani model.

The general model of the fuzzy logic controller is shown in Fig. 9. The inputs are the error of the rotor

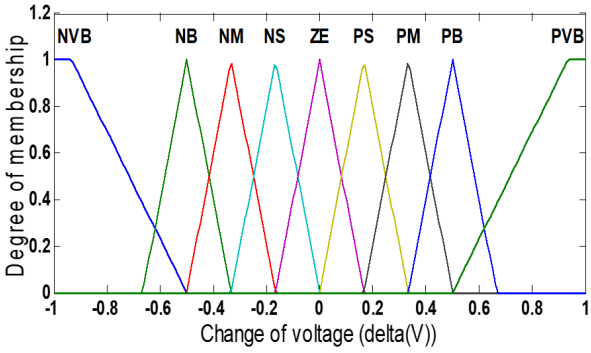

Fig. 12: *Membership functions of output ($\Delta V_{rd,q^*}$).*

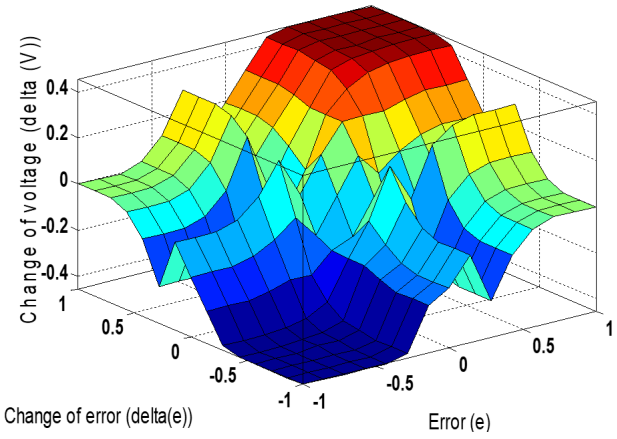

Fig. 13: *Surface of the fuzzy rules.*

Table 4: *Inference matrix of the fuzzy system.*

$\Delta V_{rd,q^*}$		e						
		NB	NM	NS	ZE	PS	PM	PB
Δe	NB	NVB	NVB	NVB	NB	NM	NS	ZE
	NM	NVB	NVB	NB	NM	NS	ZE	PS
	NS	NVB	NB	NM	NS	ZE	PS	PM
	ZE	NB	NM	NS	ZE	PS	PM	PB
	PS	NM	NS	ZE	PS	PM	PB	PVB
	PM	NS	ZE	PS	PM	PB	PVB	PVB
	PB	ZE	PS	PM	PB	PVB	PVB	PVB

current ($e_{I_{rd,q}}$) and the change error of the rotor current ($\Delta e_{I_{rd,q}}$). The output is the change in reference rotor voltage ($\Delta V_{rd,q^*}$), while $1/z$ represents the time delay [16].

The crisp inputs are converted into linguistic variables for the associated MFs, each element of which has a degree of membership ranging from zero to one. In this paper, we study the MFs of inputs (error, change of error) and output (change of voltage) as shown in Figs. 10–12.

The linguistic variables for MFs are described as follows:

- **NVB:** Negative-Very Big
- **NB:** Negative-Big
- **NM:** Negative-Medium
- **NS:** Negative-Small
- **ZE:** Zero

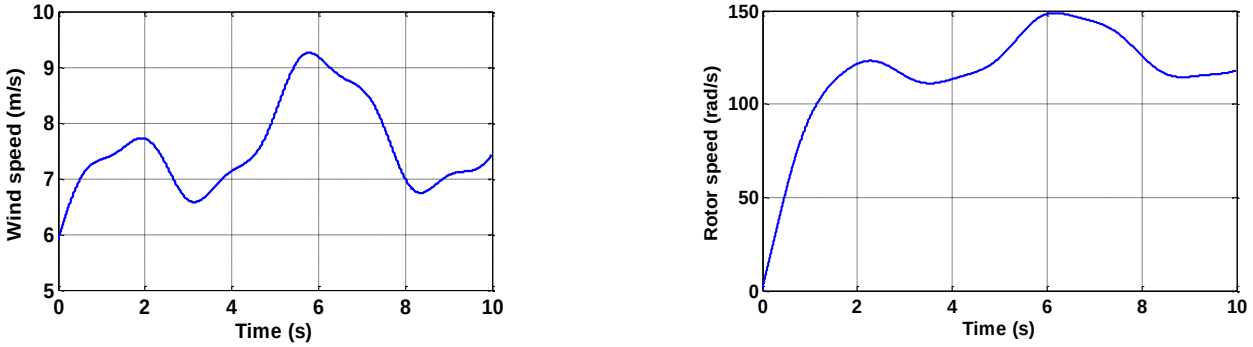

(a) (b)

Fig. 14: *(a) Wind speed and (b) rotor speed.*

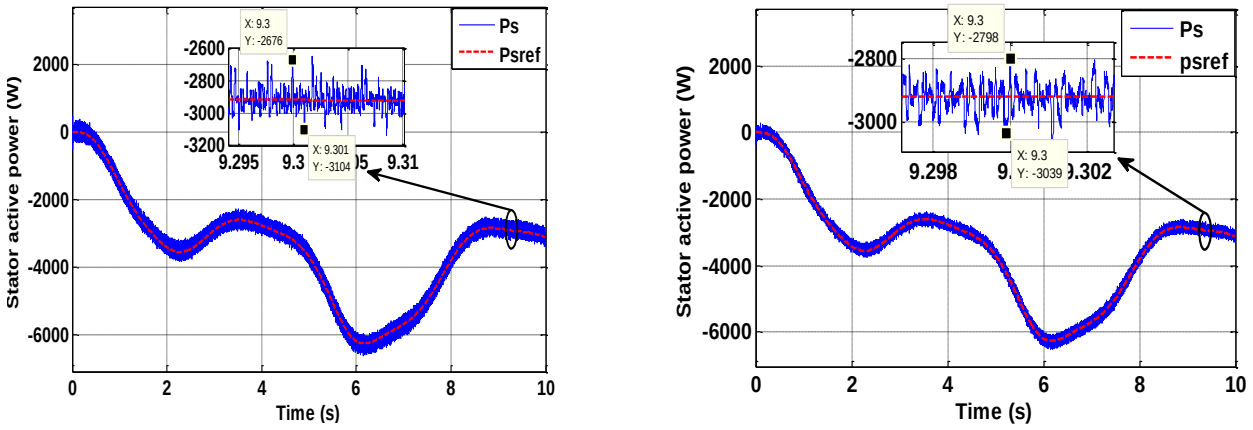

(a) (b)

Fig. 15: *Stator active power using (a) PWM and (b) SVPWM.*

- **PS:** Positive-Smell
- **PM:** Positive-Medium
- **PB:** Positive-Big
- **PVB:** Positive-Very Big.

The fuzzy inferences use the conditional rule (If…Then), between linguistic variables of inputs (e, Δe) and output ($\Delta V_{rd,q^*}$), as detailed in Table 4. The surface of the fuzzy rules is illustrated in Fig. 13.

7. SIMULATION RESULTS

Parameters of the DFIG used in this paper are as follows: $P_s = 7.5\,\text{kW}$, $R_s = 0.455\,\Omega$, $R_r = 0.62\,\Omega$, $L_s = 0.084\,\text{H}$, $L_r = 0.081\,\text{H}$, $M = 0.078\,\text{H}$, $p = 2$, $J_g = 0.3125\,\text{kg}\cdot\text{m}^2$, $f_g = 6.73 \times 10^{-3}\,\text{N}\cdot\text{m}\cdot\text{s}^{-1}$. Parameters of the wind turbine: blade radius $R = 3\,\text{m}$, rated power $P_t = 10\,\text{kW}$, gear ratio $G = 5.4$, number of blades $p = 3$, density of air $\rho = 1.22\,\text{kg/m}^3$, $J_t = 0.042\,\text{kg}\cdot\text{m}^2$, $f_t = 0.017\,\text{N}\cdot\text{m}\cdot\text{s}^{-1}$. Parameters of the total mechanical constants: $J_T = J_g + \left(J_t/G^2\right) = 0.3139\,\text{kg}\cdot\text{m}^2$, $f_T = f_g + \left(f_t/G^2\right) = 7.31 \times 10^{-3}\,\text{N}\cdot\text{m}\cdot\text{s}^{-1}$.

Fig. 14(a) shows the wind speed applied to the turbine, the value of which varies randomly from 5.9 to 9.26 m/s, over 10 s. Fig. 14(b) shows the rotor speed generated by the wind turbine being applied to the DFIG, the value of which varies from 0 to 148.83 rad/s.

Figs. 15(a) and 15(b) show the stator active power (blue line) and its reference profile (red line), the value of which varies from 0 to −6.2599 kW, integrated with the FLC using PWM and SVPWM, respectively. The reference of stator power (P_{sref}) is generated by the mechanical speed of the rotor (ω_m) multiplied by the reference of electromagnetic torque (T^*_{em}) resulting from MPPT, to obtain maximum power at all power points. Figs. 16(a) and 16(b) illustrate the stator reactive power (blue line) and its reference profile (red line) integrated with the FLC, using PWM and SVPWM, respectively. The reference value of stator reactive power is always maintained at zero ($Q_{sref} = 0$), to ensure a unit power factor (PF = 1). The simulation results revealed that SVPWM gives reduced ripples of active power ($-3039\,\text{W} \leq \Delta P_s \leq -2798\,\text{W}$) and reactive power ($-133.3\,\text{Var} \leq \Delta Q_s \leq 118.3\,\text{Var}$), compared to PWM which gives higher ripples of active power ($-3104\,\text{W} \leq \Delta P_s \leq -2676\,\text{W}$) and reactive power ($-215.2\,\text{Var} \leq \Delta Q_s \leq 192.5\,\text{Var}$).

Figs. 17(a) and 17(b) illustrate the three-phase stator currents using PWM and SVPWM, respectively. The frequency of the stator current is always constant ($f_s = 50\,\text{Hz}$) to synchronize it with the electrical grid.

Figs. 18(a) and 18(b) show a zoom of the three-phase

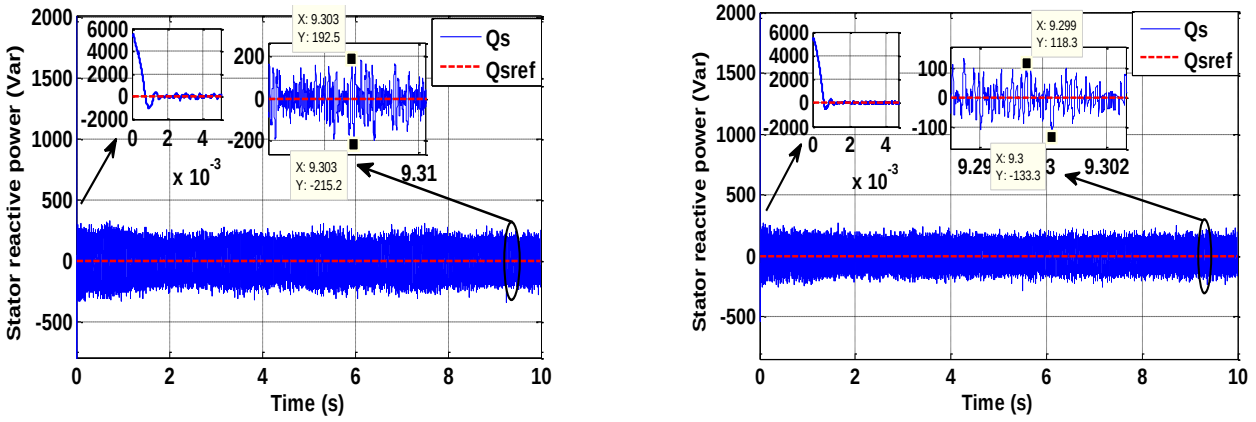

(a) (b)

Fig. 16: *Stator reactive power using (a) PWM and (b) SVPWM.*

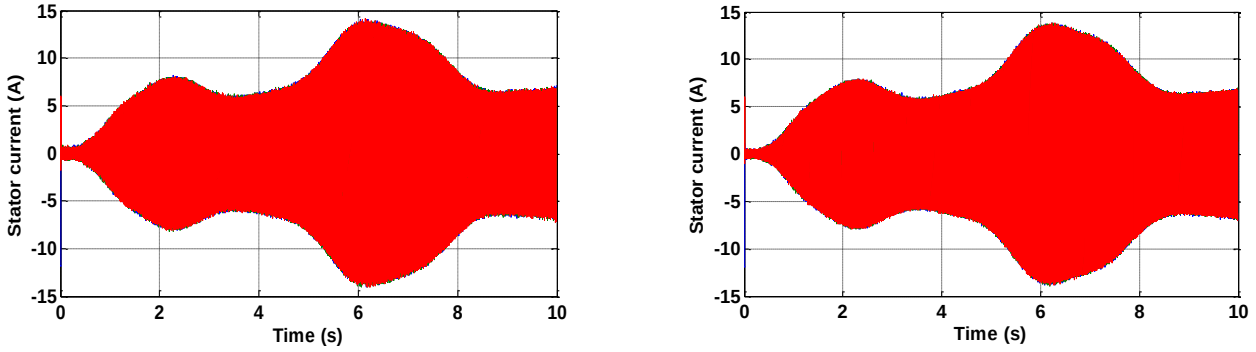

(a) (b)

Fig. 17: *Stator currents using (a) PWM and (b) SVPWM.*

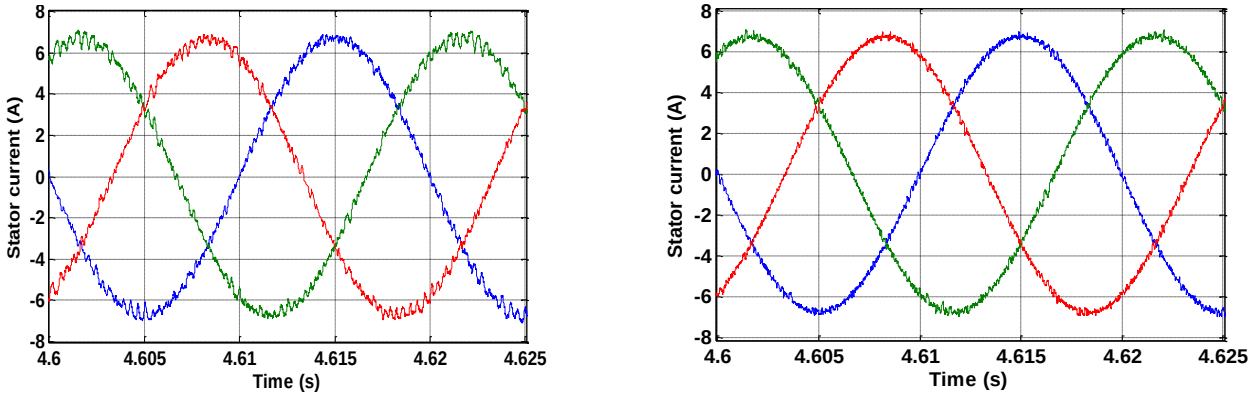

(a) (b)

Fig. 18: *Zoom of the stator currents using (a) PWM and (b) SVPWM.*

stator currents ranging between 4.6 s and 4.625 s using PWM and SVPWM, respectively. The simulation results reveal that the three-phase stator current using SVPWM has significantly lower ripples compared to PWM.

Figs. 19(a) and 19(b) illustrate the three-phase rotor currents using PWM and SVPWM, respectively. The frequency of the rotor currents relates to the rotor speed (ω_m).

Figs. 20(a) and 20(b) show a zoom of the three-phase rotor currents ranging between 2.8 s and 2.9 s using PWM and SVPWM, respectively. The simulation results reveal that the three-phase rotor current using SVPWM has lower ripples compared to PWM.

Figs. 21(a) and 21(b) show the reference rotor voltage and carrier signal using PWM and SVPWM, respectively. The simulation results reveal that the amplitude of the

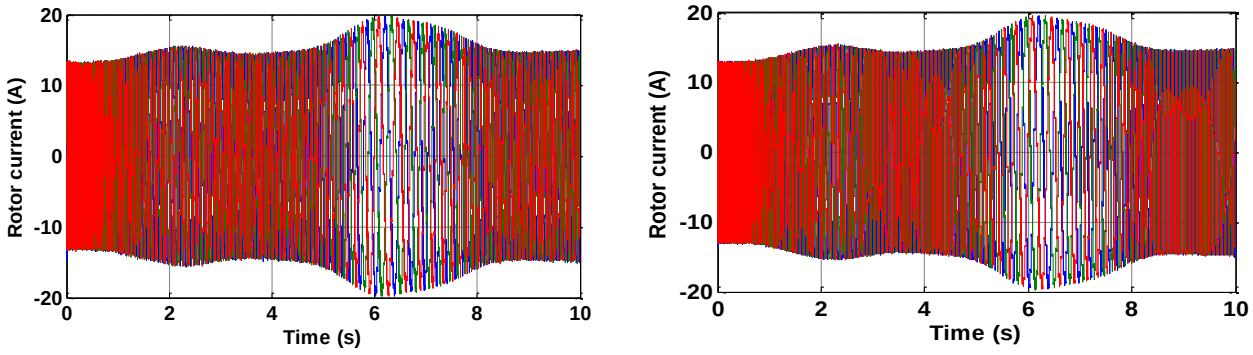

Fig. 19: *Rotor currents using (a) PWM and (b) SVPWM.*

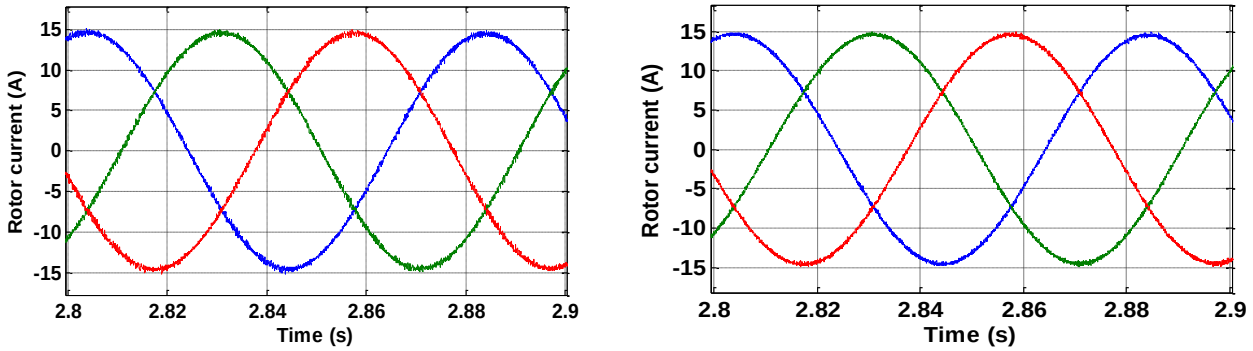

Fig. 20: *Zoom of the rotor currents using (a) PWM and (b) SVPWM.*

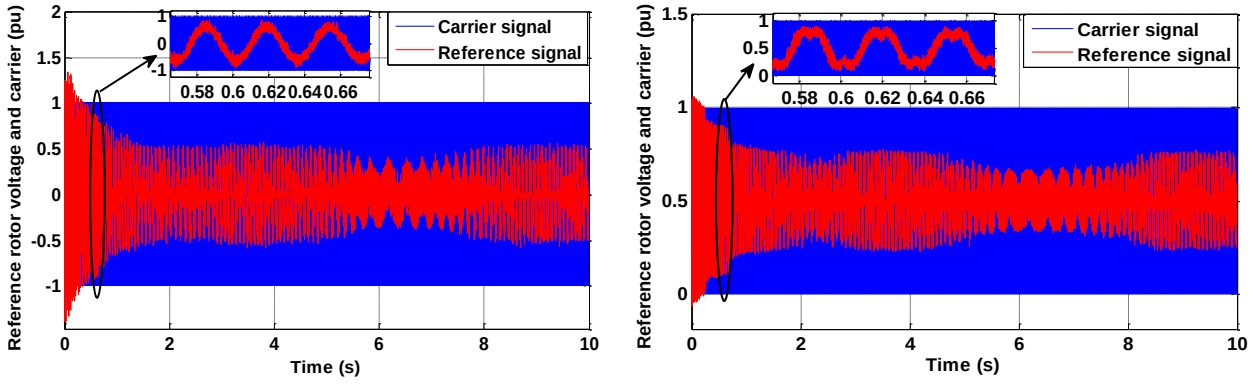

Fig. 21: *Reference rotor voltage and carrier signal using (a) PWM and (b) SVPWM.*

carrier signal is greater than or equal to the amplitude of reference signal in the permanent regime, and this should be taken into consideration to respect the control signals.

Figs. 22(a) and 22(b) present the harmonic spectrum of one phase of the stator current using PWM and SVPWM, respectively, obtained using Fast Fourier Transform (FFT). Subsequently, SVPWM had a lower THD (1.94%) compared to PWM (THD = 3.92%).

In summary, it is clear that both techniques using FLC show good tracking and greater stability in transient and non-linear systems. Furthermore, SVPWM provides better performance due to the lower ripples of active and reactive powers and reduced THD of the stator current compared to PWM.

Table 5 summarizes the performance comparison between FLC-PWM and SVPWM.

The difficulties encountered in obtaining the simulation results relate to the selection of the gains from the FLC. This is because the FLC is not subject to an arithmetic rule, and unlike the classical controller, the gains (K_e, $K_{\Delta e}$) are selected by taking into account the error ($e_{I_{rd,q}}$) and error change ($\Delta e_{I_{rd,q}}$) ripples that are

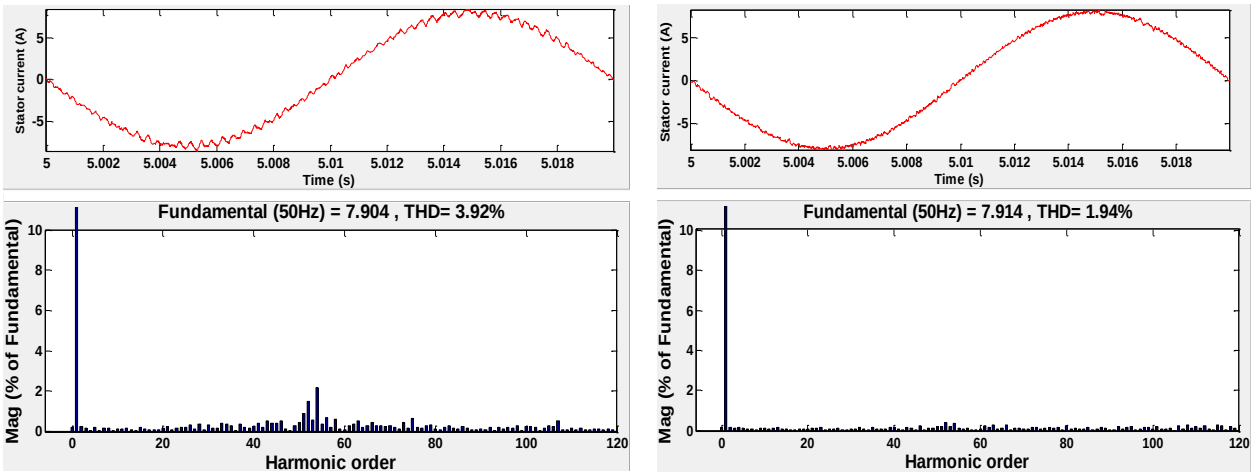

(a) (b)

Fig. 22: *Harmonic spectrum of stator current using (a) PWM and (b) SVPWM.*

Table 5: *Comparison of performance between PWM and SVPWM.*

Performance	Technique	
	FLC-PWM	FLC-SVPWM
Ripples of P_s (W)	428	241
Ripples of Q_s (Var)	407.7	251.6
THD (%)	3.92	1.94

confined to the range $[-1, 1]$. Moreover, the gain ($K_{\Delta V}$) is selected by taking into account the reference signal value (V_{rd,q^*}), the amplitude of which is less than or equal to the amplitude of the carrier signal.

A comparison of the THD value between the FLC-SVPWM proposed in this paper and other control techniques suggested in several previous articles is presented in Table 6, where SMC-PWM is the sliding mode control using a pulse width modulation inverter, SMC-SVM is the sliding mode control using a space vector modulation inverter, SMC-MC is the sliding mode control using a matrix converter, FSMC-MC is the fuzzy mode control using a matrix converter, FOC is the field-oriented control, DPC-PI-SVPWM is the direct power control with a proportional integrator controller using a space vector pulse width modulation inverter.

By comparing the results in Table 6, we found that the proposed method in this paper (FLC-SVPWM) provides better performance (lower THD (%)) compared to other control methods suggested in several previous articles.

8. CONCLUSION

A comparative study between pulse width modulation (PWM) and space vector pulse width modulation (SVPWM) based on a fuzzy logic controller (FLC) is presented in this paper for a doubly fed induction generator (DFIG) driven by a wind turbine with variable speed. Following analysis of results obtained under MATLAB/Simulink, it can be concluded that the FLC using an SVPWM inverter provides better performance than the PWM inverter, such as reduced ripples of active and reactive powers, and lower total harmonic distortion (THD) of the stator current.

Table 6: *Comparative study of the THD value between the proposed method and other control techniques.*

Reference	Control Technique	THD (%)
[17]	SMC-PWM	6.62
	SMC-SVM	2.54
[23]	SMC-MC	3.05
	FSMC-MC	2.85
[24]	FOC	3.7
[25]	DPC-PI-SVPWM	2.59
Proposed Method	FLC-SVPWM	1.94

ACKNOWLEDGMENTS

The authors would like to acknowledge support from the Directorate General for Scientific Research and Technological Development (DGRSDT), Ministry of Higher Education and Scientific Research – Algeria.

REFERENCES

[1] H. Karimi-Davijani, A. Sheikholeslami, H. Livani, and M. Karimi-Davijani, "Fuzzy logic control of doubly fed induction generator wind turbine," *World Applied Sciences Journal*, vol. 6, no. 4, pp. 499–508, 2009.

[2] E. Artigao, A. Honrubia-Escribano, and E. Gomez-Lazaro, "In-service wind turbine DFIG diagnosis using current signature analysis," *IEEE Transactions on Industrial Electronics*, vol. 67, no. 3, pp. 2262–2271, Mar. 2020.

[3] S. S. Yu, G. Zhang, T. Fernando, and H. H.-C. Iu, "A DSE-based SMC method of sensorless DFIG

wind turbines connected to power grids for energy extraction and power quality enhancement," *IEEE Access*, vol. 6, pp. 76 596–76 605, 2018.

[4] D. Thakur and J. Jiang, "Control of a PMSG wind-turbine under asymmetrical voltage sags using sliding mode approach," *IEEE Power and Energy Technology Systems Journal*, vol. 5, no. 2, pp. 47–55, Jun. 2018.

[5] M. E. Azzaoui and H. Mahmoudi, "Fuzzy-PI control of a doubly fed induction generator-based wind power system," *International Journal of Automation and Control*, vol. 11, no. 1, pp. 54–66, 2017.

[6] S. Benelghali, M. Benbouzid, and J. F. Charpentier, "DFIG versus PMSG for marine current turbine applications," *Revue des Energies Renouvelables*, vol. 15, no. 1, pp. 29–41, 2012.

[7] Z. Zhang, Y. Zhao, W. Qiao, and L. Qu, "A space-vector-modulated sensorless direct-torque control for direct-drive PMSG wind turbines," *IEEE Transactions on Industry Applications*, vol. 50, no. 4, pp. 2331–2341, Jul. 2014.

[8] N. Govindarajan and D. Raghavan, "Doubly fed induction generator based wind turbine with adaptive neuro fuzzy inference system controller," *Asian Journal of Scientific Research*, vol. 7, no. 1, pp. 45–55, 2014.

[9] I. Idrissi, H. Chafouk, R. E. Bachtiri, and M. Khanfara, "Modeling and simulation of the variable speed wind turbine based on a doubly fed induction generator," in *Modeling of Turbomachines for Control and Diagnostic Applications*, I. Loboda and S. Yepifanov, Eds. IntechOpen, 2019.

[10] Y. Bai, B. Kou, and C. C. Chan, "A simple structure passive MPPT standalone wind turbine generator system," *IEEE Transactions on Magnetics*, vol. 51, no. 11, pp. 1–4, Nov. 2015.

[11] J. S. Thongam and M. Ouhrouche, "MPPT control methods in wind energy conversion systems," in *Fundamental and Advanced Topics in Wind Power*, R. Carriveau, Ed. IntechOpen, 2011, pp. 339–360.

[12] X. Du and H. Yin, "MPPT control strategy of DFIG-based wind turbines using double steps hill climb searching algorithm," in *2015 5th International Conference on Electric Utility Deregulation and Restructuring and Power Technologies (DRPT)*. Changsha, China, 26–29 Nov. 2015, pp. 1910–1914.

[13] F. Fateh, W. N. White, and D. Gruenbacher, "A maximum power tracking technique for grid-connected DFIG-based wind turbines," *IEEE Journal of Emerging and Selected Topics in Power Electronics*, vol. 3, no. 4, pp. 957–966, Dec. 2015.

[14] L. A. Zadeh, "Fuzzy sets," *Information and Control*, vol. 8, no. 3, pp. 338–353, Jun. 1965.

[15] Y. Bai and D. Wang, "Fundamentals of fuzzy logic control — fuzzy sets, fuzzy rules and defuzzifications," in *Advanced Fuzzy Logic Technologies in Industrial Applications*, Y. Bai, H. Zhuang, and D. Wang, Eds. London, UK: Springer, 2006, pp. 17–36.

[16] M. R. Hazari, M. A. Mannan, S. M. Muyeen, A. Umemura, R. Takahashi, and J. Tamura, "Stability augmentation of a grid-connected wind farm by fuzzy-logic-controlled DFIG-based wind turbines," *Applied Sciences*, vol. 8, no. 1, 2018, Art. no. 20.

[17] Y. Bekakra and D. B. Attous, "DFIG sliding mode control driven by wind turbine with using a svm inverter for improve the quality of energy injected into the electrical grid," *ECTI Transactions on Electrical Engineering, Electronics, and Communications*, vol. 11, no. 1, pp. 63–75, Feb. 2013.

[18] Y. Bekakra and D. B. Attous, "Optimal tuning of PI controller using PSO optimization for indirect power control for DFIG based wind turbine with MPPT," *International Journal of System Assurance Engineering and Management*, vol. 5, no. 3, pp. 219–229, 2014.

[19] J. Ouyang, T. Tang, J. Yao, and M. Li, "Active voltage control for DFIG-based wind farm integrated power system by coordinating active and reactive powers under wind speed variations," *IEEE Transactions on Energy Conversion*, vol. 34, no. 3, pp. 1504–1511, Sep. 2019.

[20] Y.-C. Liu, X.-L. Ge, X.-Y. Feng, and R.-J. Ding, "Relationship between SVPWM and carrier-based PWM of eight-switch three-phase inverter," *Electronics Letters*, vol. 51, no. 13, pp. 1018–1019, Jun. 2015.

[21] G. Vivek, J. Biswas, M. D. Nair, and M. Barai, "Simplified double switching SVPWM implementation for three-level VSI," *The Journal of Engineering*, vol. 2019, no. 11, pp. 8257–8269, Nov. 2019.

[22] A. Y. Yousef, "Space vector pulse width modulation technique," *International Journal of Emerging Technology in Computer Science & Electronics*, vol. 15, no. 1, pp. 159–165, May 2015.

[23] Z. Boudjema, A. Meroufel, Y. Djerriri, and E. Bounadja, "Fuzzy sliding mode control of a doubly fed induction generator for wind energy conversion," *Carpathian Journal of Electronic and Computer Engineering*, vol. 6, no. 2, pp. 7–14, 2013.

[24] F. Amrane, A. Chaiba, B. E. Babes, and S. Mekhilef, "Design and implementation of high performance field oriented control for grid-connected doubly fed induction generator via hysteresis rotor current controller," *Revue Roumaine des Sciences Techniques, Série Électrotechnique et Énergétique*, vol. 61, no. 4, pp. 319–324, 2016.

[25] H. Benbouhenni, A. Belaidi, and Z. Boudjema, "Power ripple reduction of DPC DFIG drive using ANN controller," *Acta Electrotechnica et Informatica*, vol. 20, no. 1, pp. 15–22, 2020.

Abdelhalim Arif received the B.Sc. degree in Electrical Engineering from Ouargla University, Algeria in 2011, and Master's degree from Batna University, Algeria in 2013. In 2015, he made his first recording to prepare his PhD in Electrical Engineering from El Oued University, Algeria. His research areas are about renewable energies, especially wind energy based on DFIG using advanced technologies under grid voltage dips.

Youcef Bekakra received the B.Sc. degree in Electrical Engineering from El Oued University, Algeria in 2007, and M.Sc. degree from El Oued University in 2010. In 2011, he was recruited as Assistant Professor at the University of El Oued, Algeria. In 2014, he received his PhD degree in Electrical Engineering from Biskra University, Algeria. He was promoted to Full Professor in July 2021. His areas of interest are Electrical Drives and Process Control, renewable energy, application of Artificial Intelligence techniques. He is a member of the LEVRES Research Laboratory.

Djilani Ben Attous received his Engineering degree in Electrotechnics from Polytechnic National Institute Algiers, Algeria in 1984, and M.Sc. degree in Power Systems from University of Manchester Institute of Science and Technology (UMIST), UK in 1987. In 2000, he received his doctorate of state (PhD degree) from Batna University, Algeria. He is currently an associate professor at El Oued University, Algeria in Electrical Engineering. His research interests in Planning and Economic of Electric Energy System, Optimization Theory and its applications and he also investigated questions related to Electrical Drives and Process Control. He is a member of the VTRS Research Laboratory.